

Nanoparticle-mediated controlled entanglement based on non-Hermitian couplingZhong-Hui Yuan,¹ Zhang Geng,¹ Yong-Jian Chen,¹ Yan Xia,² Yong-Yuan Jiang ,¹ and Jie Song^{1,3,4,5,*}¹*School of Physics, Harbin Institute of Technology, Harbin 150001, China*²*Department of Physics, Fuzhou University, Fuzhou 350002, China*³*Key Laboratory of Micro-Nano Optoelectronic Information System, Ministry of Industry and Information Technology, Harbin 150001, China*⁴*Key Laboratory of Micro-Optics and Photonic Technology of Heilongjiang Province, Harbin Institute of Technology, Harbin 150001, China*⁵*Collaborative Innovation Center of Extreme Optics, Shanxi University, Taiyuan, Shanxi 030006, China*

(Received 20 January 2024; accepted 30 July 2024; published 27 August 2024)

We propose a method to achieve a coherent switch of optomagnonic entanglement in a cavity optomagnonic system with non-Hermitian coupling. The strength of photon-photon and photon-magnon entanglement can be controlled by tuning the relative phase angle of two nanoparticles and optimizing the detuning of two optical modes. We show that the bipartite entanglement is significantly enhanced by selecting a suitable optomagnonics coupling strength in the presence of the exceptional points (EPs). The relative phase not only enhances the entanglement strength but also increases the entanglement domain over a wide range of detuning compared to the Hermitian system. By manipulating the system toward or away from EPs, versatile tunability of the tripartite entanglement, mean photon, and magnon numbers can be achieved. Additionally, the direction of asymmetric transmission can also be well tuned in a highly asymmetric way via non-Hermitian coupling. The study of controlled entanglement may provide the theoretical basis and reference for the research and development of new tunable quantum devices.

DOI: [10.1103/PhysRevA.110.023732](https://doi.org/10.1103/PhysRevA.110.023732)**I. INTRODUCTION**

Cavity optomagnonics describes the hybrid interaction between the optical field and the magnetic field in microresonators [1–11]. Spin waves are an essential information carrier in contemporary information technology because they describe the collective excitation of magnetization in ordered magnets and can propagate without the directional motion of electrons. Recent experiments have shown that an yttrium iron garnet (YIG) sphere has extremely high spin density and long coherence time, which results in strong and even ultrastrong coupling with microwave photons and optical photons. The coupled dynamics of magnons and photons in the optical regime can lead to coherent manipulation of magnons with light. The origin of this magnon-photon interaction is the Faraday effect, in which the angle of polarization of the light changes as it propagates through a magnetic material [12]. YIG sphere serves as the host of the magnetic excitations and, via whispering-gallery modes (WGM), as the optical cavity [13–17]. Very recent experiments in this regime showed that this is a promising route by demonstrating coupling between optical modes and magnons, and advances in this field are expected to develop rapidly.

The study of magneto-optical-effect setups also enables in-depth examination of quantum phenomena in hybrid optomagnonic systems, allowing for the observation of rich quantum effects. Quantum entanglement [18,19], one of the most intrinsic properties of quantum mechanics, corresponds

to a valuable resource for quantum information processing, such as performing computation and secure communication. Beyond bipartite quantum entanglement, multipartite entanglement can offer a more fundamental resource for a wide range of quantum information-processing tasks, and thus, they can be used for future quantum technologies, such as the quantum internet and programmable quantum networks [20]. Recently, with the rapid development of nanotechnology, the introduction of nano-objects into microcavities has spawned prospective new technologies with widespread applications [21]. More importantly, exceptional points, at which the eigenvalues and the corresponding eigenvectors of the system coalesce, have been observed experimentally in such coupled optical systems, and several counterintuitive phenomena related to exceptional points have been investigated deeply [22,23].

A previous experiment demonstrated that nanoparticles as a scatterer in WGM microresonators can induce asymmetric backscattering of optical-field propagation, and in the vicinity of an exceptional point, the mode exhibits strong chiral behavior [24–33]. Non-Hermitian theory is one of the most fascinating properties of asymmetry and has fundamental implications in several branches of modern physics, such as the quantum Hall effect, the topological magnon Hall effect [34–38], and chiral p -wave superconductors [39–41]. Recently, relevance theory also suggested that tuning the relative position of nanoparticles not only can result in frequency combs and periodic photon-magnon blockade [42,43] but can also significantly change the transmission spectrum in the vicinities of exceptional points (EPs) [44–49]. Motivated by recent experiments, here, we transfer non-Hermitian concepts

*Contact author: jsong@hit.edu.cn

to controlled quantum entanglement in an optomagnonics microresonator. Natural questions when we consider a system consisting of a YIG microresonator coupled to two silica nanoparticles are whether the optomagnonics entanglement is controlled by the presence of the relative phase angle and whether this effect can be used to achieve periodic tripartite entanglement and asymmetric transmission. The study of controlled optomagnonics entanglement may promote the intersection and merging of various disciplines, such as non-Hermitian physics, and provide the theoretical basis and reference for the research and development of new tunable quantum devices.

In the present work, we propose to achieve nanoparticle-mediated control of steady light-magnon entanglement in a non-Hermitian cavity optomagnonics system, and then we show its robustness against the relative phase angle corresponding to optical backscattering. Specifically, we consider a cavity optomagnonics system supporting a YIG sphere coupled to two nanoparticles that is coherently driven by an input field. With careful variation of the relative positions of the nanoparticles, the coupling of optical modes changes periodically, and the eigenvalues of the cavity optomagnonics system coalesce at the EPs. Under the joint effect of the scatterers, steady-state entanglement and transmission can be significantly controlled, which benefits from the modification of the non-Hermitian character of the system. We find that a coherent asymmetric switch of controlled entanglement can be implemented by properly regulating the relative phase angle. Particularly, it is shown that controlled entanglement tends to be enhanced in the vicinity of EPs, implying that nanoparticles are helpful for preserving the coherence of quantum systems. We can see that, with a suitable optomagnonics coupling strength, the bipartite entanglement of the cavity optomagnonics system increases dramatically. And the direction of asymmetric transmission can also be well tuned in a highly asymmetric way via non-Hermitian coupling. Additionally, we reveal the versatile tunability of the tripartite optomagnonics entanglement and the mean photon and magnon numbers by manipulating the system toward or away from EPs.

II. SYSTEM AND HAMILTONIAN

As Fig. 1 depicts, we consider a system consisting of a YIG microresonator coupled to two silica nanoparticles, engineered by wet etching of a tapered fiber. Here, we assume that optical clockwise (CW) and counterclockwise (CCW) modes are excited simultaneously in the resonator, in which they are coupled with the YIG sphere. The corresponding coupling dynamics relies on the Faraday effect; when light propagates in a magnetic material, the polarization direction of the light will change. The nanoparticles are placed in the evanescent field of the YIG resonator, and their positions can be adjusted. The non-Hermitian coupling between the CW and CCW modes is tuned by controlling the relative size and position of two nanoparticles or Rayleigh scatterers placed within the mode volume of the microresonator. The coupling strength can be approximately treated as $J_{12(21)} = \epsilon_1 + \epsilon_2 e^{\pm i\sigma\beta}$, where $\epsilon_{1(2)}$ are given by the complex frequency shifts for positive-parity and negative-parity modes introduced by only the particles S_1 and S_2 . They can be changed by adjusting the position and

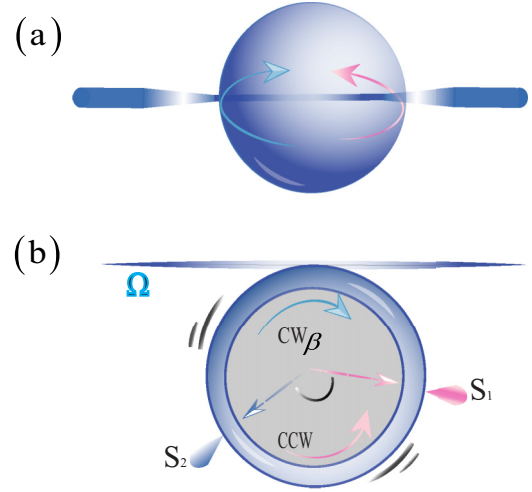


FIG. 1. Schematic diagram of the cavity optomagnonic system consisting of a YIG sphere coupled with two nanoparticles. The homogeneous magnon mode couples to the optical modes with strength g_j . The relative angle between the two nanotips $S_{1,2}$ is denoted by β , and the scattering rate of backscattering from the CW (CCW) to CCW (CW) mode is characterized by $J_{12,21}$.

size of the nanoparticles. σ is the azimuthal mode number, and β is the relative phase angle between two nanoparticles. The first nanoparticle induces a symmetric coupling between the CW and CCW modes and lifts their frequency degeneracy, leading to mode splitting. The second nanoparticle then breaks this symmetry, leading to periodic EPs that emerge as the relative angle between the nanoparticle along the boundary of the resonator is varied. Such a model of the hybrid cavity optomagnonic system can be described by a non-Hermitian interaction Hamiltonian,

$$H_1 = \omega_{\odot} \hat{a}_{\odot}^{\dagger} \hat{a}_{\odot} + \omega_{\ominus} \hat{a}_{\ominus}^{\dagger} \hat{a}_{\ominus} + \omega_m \hat{m}^{\dagger} \hat{m} + K \hat{m}^{\dagger} \hat{m} \hat{m}^{\dagger} \hat{m} + g_1 \hat{a}_{\odot}^{\dagger} \hat{a}_{\odot} (\hat{m}^{\dagger} + \hat{m}) + g_2 \hat{a}_{\ominus}^{\dagger} \hat{a}_{\ominus} (\hat{m}^{\dagger} + \hat{m}) + J_{12} \hat{a}_{\odot}^{\dagger} \hat{a}_{\ominus} + J_{21} \hat{a}_{\ominus} \hat{a}_{\odot}^{\dagger} + \Omega (\hat{a}_{\odot}^{\dagger} e^{-i\omega_l t} + \hat{a}_{\ominus}^{\dagger} e^{-i\omega_l t} + \text{H.c.}), \quad (1)$$

where \hat{a}_j (\hat{a}_j^{\dagger}) is the annihilation (creation) operator for optical modes with frequency ω_j ($j = \odot, \ominus$, indexing the CW and CCW directions, respectively) and \hat{m} is the annihilation operator for a magnon mode with fundamental frequency ω_m . Specifically, there is coherent coupling between the CW (CCW) mode \hat{a}_1 and (\hat{a}_2) and the magnon mode \hat{m} , corresponding to coupling strengths g_1 and (g_2). The system is driven by a weak pump field with drive amplitude Ω and frequency ω_l . Then, in the rotating frame with respect to the driving laser field $V = \exp[-i\omega_l t (\hat{a}_{\odot}^{\dagger} \hat{a}_{\odot} + \hat{a}_{\ominus}^{\dagger} \hat{a}_{\ominus})]$, the total Hamiltonian of the system can be reduced to

$$H' = \Delta_{\odot} \hat{a}_{\odot}^{\dagger} \hat{a}_{\odot} + \Delta_{\ominus} \hat{a}_{\ominus}^{\dagger} \hat{a}_{\ominus} + \omega_m \hat{m}^{\dagger} \hat{m} + K \hat{m}^{\dagger} \hat{m} \hat{m}^{\dagger} \hat{m} + g_1 \hat{a}_{\odot}^{\dagger} \hat{a}_{\odot} (\hat{m}^{\dagger} + \hat{m}) + g_2 \hat{a}_{\ominus}^{\dagger} \hat{a}_{\ominus} (\hat{m}^{\dagger} + \hat{m}) + J_{12} \hat{a}_{\odot}^{\dagger} \hat{a}_{\ominus} + J_{21} \hat{a}_{\ominus} \hat{a}_{\odot}^{\dagger} + \Omega (\hat{a}_{\odot}^{\dagger} + \hat{a}_{\ominus}^{\dagger} + \text{H.c.}). \quad (2)$$

Assuming the frequency of the CW mode is equal to that of the CCW mode, i.e., $\omega_{\odot} = \omega_{\ominus} = \omega$, the detuning of the optical mode is given by $\Delta_j = \omega_j - \omega_l$ ($j = \odot, \ominus$, indexing the CW and CCW directions, respectively).

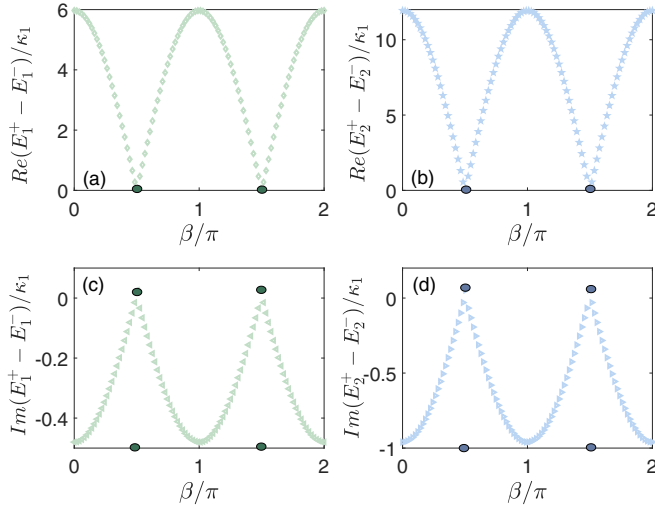


FIG. 2. Real parts of the frequency splitting, (a) $\text{Re}(E_1^+ - E_1^-)/\kappa_1$ and (b) $\text{Re}(E_2^+ - E_2^-)/\kappa_1$, varying with the angle β . Imaginary parts of the frequency splitting, (c) $\text{Im}(E_1^+ - E_1^-)/\kappa_1$ and (d) $\text{Im}(E_2^+ - E_2^-)/\kappa_1$, varying with the angle β . The parameters are set as $\epsilon_1/\kappa = 1.5 - i0.1$, $\epsilon_2/\kappa = 1.485 - i0.14$, $\sigma = 1$, and $\chi/\kappa_1 = 5$.

III. EIGENENERGY SPECTRUM OF THE CAVITY OPTOMAGNONIC SYSTEM AND ASYMMETRIC BACKSCATTERING AT EPs

Consider a polaron transformation $U = \exp[g/\omega_m(\hat{a}_\circ^\dagger \hat{a}_\circ + \hat{a}_\circ^\dagger \hat{a}_\circ)(m^\dagger - m)]$ the transformed Hamiltonian $H_{\text{eff}} = U^\dagger H' U$ can be rewritten as

$$H_{\text{eff}} = \Delta_\circ \hat{a}_\circ^\dagger \hat{a}_\circ + \Delta_\circ \hat{a}_\circ^\dagger \hat{a}_\circ + \omega_m \hat{m}^\dagger \hat{m} + K \hat{m}^\dagger \hat{m} \hat{m}^\dagger \hat{m} + g_1^2/\omega_m [(\hat{a}_\circ^\dagger \hat{a}_\circ)^2 + (\hat{a}_\circ^\dagger \hat{a}_\circ)^2 + 2(\hat{a}_\circ^\dagger \hat{a}_\circ \hat{a}_\circ^\dagger \hat{a}_\circ)] + J_{12} \hat{a}_\circ^\dagger \hat{a}_\circ + J_{21} \hat{a}_\circ \hat{a}_\circ^\dagger + \Omega(\hat{a}_\circ^\dagger + \hat{a}_\circ + \text{H.c.}), \quad (3)$$

with $\chi = g_1^2/\omega_m$; some exponential factors have been approximately omitted under the condition of weak optomechanical coupling $g_1/\omega_m \ll 1$. This Hamiltonian indicates that the magnon mode has been decoupled from the optical modes; namely, the evolutions of the optical and magnon parts are independent of each other. In Hamiltonian (3), the magnon part can be ignored in that we care about only the optical properties of the system; then the reduced effective Hamiltonian reads

$$H'_{\text{eff}} = \Delta_\circ \hat{a}_\circ^\dagger \hat{a}_\circ + \Delta_\circ \hat{a}_\circ^\dagger \hat{a}_\circ + J_{12} \hat{a}_\circ^\dagger \hat{a}_\circ + J_{21} \hat{a}_\circ \hat{a}_\circ^\dagger + \chi [(\hat{a}_\circ^\dagger \hat{a}_\circ)^2 + (\hat{a}_\circ^\dagger \hat{a}_\circ)^2 + 2(\hat{a}_\circ^\dagger \hat{a}_\circ \hat{a}_\circ^\dagger \hat{a}_\circ)] + \Omega(\hat{a}_\circ^\dagger + \hat{a}_\circ + \text{H.c.}). \quad (4)$$

To gain more insight into controlled entanglement, we investigate the eigenenergy of the non-Hermitian Hamiltonian, as shown in Fig. 2. In the weak-driving regime, the Hilbert space of this system can be restricted to a subspace with a few photons spanned by the basis states with the total excitation number which denotes the Fock state with n_1 photons in the bare CW mode and n_2 photons in the CCW mode. In the single-excitation subspace, we write the eigenenergies of the non-Hermitian Hamiltonian (4) without the driving term

as

$$E_1^\pm = \omega + \chi + \lambda_1^\pm, \quad (5)$$

with the corresponding non-normalized eigenstates

$$|\psi_1^\pm\rangle = \pm\sqrt{J_{12}}|0, 1\rangle + \sqrt{J_{21}}|1, 0\rangle, \quad (6)$$

where $\lambda_1^\pm = \pm\sqrt{J_{12}J_{21}}$. Moreover, we also obtain the eigenenergies $E_2^s = 2\omega + 4\chi + \lambda_2^s$ and corresponding non-normalized eigenstates $|\psi_2^\pm\rangle = \sqrt{2}J_{12}|0, 2\rangle + \lambda_2^\pm|1, 1\rangle + \sqrt{2}J_{21}|2, 0\rangle$ and $|\psi_2^0\rangle = J_{12}|0, 2\rangle + J_{21}|2, 0\rangle$ in the two-excitation subspace, where $s = \pm, 0$, $\lambda_2^\pm = \pm 2\sqrt{J_{12}J_{21}}$, and $\lambda_2^0 = 0$. This shows that the eigenmode structure depending on the asymmetry of the coupling coefficients J_{12} and J_{21} can be tuned by controlling the relative angular position β between the nanoparticles. Therefore, the relative positions of nanoparticles have an important effect on the non-Hermitian property.

Different from the degeneracy of eigenenergies, EPs correspond to the situation where the two eigenenergies and their eigenstates coalesce. To find EPs of the non-Hermitian system, we plot the real and imaginary parts of the frequency splitting as a function of β , as shown in Fig. 2, which shows H_{eff} has two EPs with energy $E_1^\pm = \omega + \chi$. In this case, EPs emerge when $E_1^+ = E_1^-$, which leads to J_{12} or J_{21} equaling zero. For $J_{12} = J_{21} = 0$, i.e., when the two nanoscatterers are absent, the Hamiltonian H' has two orthogonal eigenstates with the same frequency. For $J_{12} = 0$ or $J_{21} = 0$, H_{eff} has only one eigenvalue and one eigenvector, indicating the emergence of an EP. In this case, when $J_{12} = 0$, we have

$$\beta_{\text{EPs}} = \frac{l\pi}{2\sigma} \pm \frac{\arg(\epsilon_1) - \arg(\epsilon_2)}{2\sigma}, \quad l = \pm 1, \pm 3, \dots, \quad (7)$$

where $\epsilon_1/\epsilon_1^* \neq \epsilon_2/\epsilon_2^*$ can be achieved in experiments by tuning the distance between the resonator and the particles and \pm corresponds to $J_{12} = 0$ or $J_{21} = 0$. The EPs also exhibit a completely asymmetric coupling between the CW and CCW modes, meaning that light can only scatter from the CCW mode to the CW mode when $J_{12} = 0$ and $J_{21} \neq 0$ and from the CW mode to the CCW mode when $J_{12} \neq 0$ and $J_{21} = 0$. Since the coupling between optical modes is dependent on the relative angular position β of the two nanoscatterers, adjusting β allows the system to be placed at EPs. We show that asymmetric backscattering, or light scattering with a different strength from the clockwise to the counterclockwise propagation direction, is generally caused by the evanescent coupling of two or more nanoparticles. The mode structure can be significantly affected by asymmetric backscattering, even in cases where its strength is weak. In non-Hermitian systems, the eigenfrequency of resonance modes coalesces at the EPs in the frequency domain, leading to extraordinary parametric sensitivity.

IV. DISSIPATIVE EQUATIONS AND COVARIANCE MATRIX

From the Hamiltonian (2), the Heisenberg-Langevin equations of the systems can be described by including the dissipation and input noise of each mode; they are given

by

$$\begin{aligned}
\dot{\hat{a}}_{\circ} &= -(i\Delta_{\circ} + \kappa_1)\hat{a}_{\circ} - ig_1\hat{a}_{\circ}(\hat{m} + \hat{m}^{\dagger}) - iJ_1\hat{a}_{\circ} \\
&\quad - i\Omega + \sqrt{2\kappa_1}\hat{a}_{\circ}^{\text{in}}, \\
\dot{\hat{a}}_{\ominus} &= -(i\Delta_{\circ} + \kappa_2)\hat{a}_{\ominus} - ig_2\hat{a}_{\ominus}(\hat{m} + \hat{m}^{\dagger}) - iJ_2\hat{a}_{\ominus} \\
&\quad - i\Omega + \sqrt{2\kappa_2}\hat{a}_{\ominus}^{\text{in}}, \\
\dot{\hat{m}} &= -(i\omega_m + \gamma_m)\hat{m} - ig_1\hat{a}_{\circ} - ig_2\hat{a}_{\ominus} - 2iK\hat{m}^{\dagger}\hat{m}\hat{m} \\
&\quad + \sqrt{2\gamma_m}\hat{m}^{\text{in}}, \tag{8}
\end{aligned}$$

where κ_1 , κ_2 , and γ_m are the damping rates of the optical modes and the magnon mode and \hat{a}_j^{in} and \hat{m}^{in} represent the input noises of the three modes. The corresponding noise operators $\hat{a}_{\circ}^{\text{in}}$, $\hat{a}_{\ominus}^{\text{in}}$, and \hat{m}^{in} satisfy the following time correlations:

$$\begin{aligned}
\langle \hat{a}_j^{\text{in}}(t)\hat{a}_j^{\text{in}\dagger}(t') \rangle &= (N_j + 1)\delta(t - t'), \\
\langle \hat{a}_j^{\text{in}\dagger}(t')\hat{a}_j^{\text{in}}(t) \rangle &= N_j\delta(t - t'), \\
\langle \hat{m}_{\text{in}}(t)\hat{m}_{\text{in}}^{\dagger}(t') \rangle &= (N_m + 1)\delta(t - t'), \\
\langle \hat{m}_{\text{in}}^{\dagger}(t)\hat{m}_{\text{in}}(t') \rangle &= N_m\delta(t - t'), \tag{9}
\end{aligned}$$

where $N_{j(m)} = (e^{\frac{\hbar\omega_j(m)}{k_B T}} - 1)^{-1}$ is the equilibrium mean number of the thermal photon and magnon occupancy under the environmental temperature T and the Boltzmann constant k_B . Since the optical mode is strongly driven, this leads to a large amplitude, $|\langle \hat{\rho} \rangle| \gg 1$. This allows us to linearize the system dynamics around the classical average values by writing the mode operators as $\hat{a}_{\circ} = A_{\circ} + a_{\circ}$, $\hat{a}_{\ominus} = A_{\ominus} + \delta a_{\circ}$, and $\hat{m} = M + m$, where the displaced operators a_{\circ} , a_{\ominus} , and m represent quantum fluctuations of these three modes, respectively, around their respective classical values A_{\circ} , A_{\ominus} , and M . The equations for the classical averages in the steady state are as follows:

$$\begin{aligned}
0 &= -(i\Delta_{\circ} + \kappa_1)A_{\circ} - ig_1(M + M^*) - iJ_1A_{\circ} - i\Omega, \\
0 &= -(i\Delta_{\circ} + \kappa_2)A_{\ominus} - ig_2(M + M^*) - iJ_2A_{\circ} - i\Omega, \\
0 &= -(i\omega_m + \gamma_m)M - ig_1|A_{\circ}|^2 - ig_2|A_{\circ}|^2 \\
&\quad - 2iK|M|^2M. \tag{10}
\end{aligned}$$

Supposing $|\Delta_{\circ}| \gg \kappa_1$ and $|\Delta_{\circ}| \gg \kappa_2$, we can approximately find that $\langle A_{\circ} \rangle$, $\langle A_{\ominus} \rangle$, and $\langle M \rangle$ are all pure real numbers. It should be noted that the approximation is used only to

demonstrate that $\langle A_{\circ} \rangle$, $\langle A_{\ominus} \rangle$, and $\langle M \rangle$ are approximately real numbers, which simplifies the following calculations.

The linearized quantum Langevin equations (QLEs) for the quantum fluctuations can be written as

$$\begin{aligned}
\frac{da_{\circ}}{dt} &= -(i\Delta_{\circ} + \kappa_1)a_{\circ} - iG_{\circ}(m + m^{\dagger}) - iJ_1a_{\circ} \\
&\quad - ig_1a_{\circ}(M + M^*), \\
\frac{da_{\ominus}}{dt} &= -(i\Delta_{\circ} + \kappa_2)a_{\ominus} - iG_{\circ}(m + m^{\dagger}) - iJ_2a_{\circ} \\
&\quad - ig_1a_{\circ}(M + M^*), \\
\frac{dm}{dt} &= -(i\Delta_m + \gamma_m)m - iG_{\circ}(a_{\circ} + a_{\circ}^{\dagger}) \\
&\quad - iG_{\circ}(a_{\circ} + a_{\circ}^{\dagger}) - 2iK|M|^2m^{\dagger}, \tag{11}
\end{aligned}$$

where $\Delta_m = \omega_m + 4K|M|^2$, $G_{\circ} = g_1A_{\circ}$, and $G_{\ominus} = g_2A_{\circ}$. To quantify the entanglement of the system, we introduce the quadrature fluctuation (noise) operators $X_o = (o + o^{\dagger})/\sqrt{2}$, $Y_o = i(o^{\dagger} - o)/\sqrt{2}$, $X_o^{\text{in}} = (o^{\text{in}} + o^{\text{in}\dagger})/\sqrt{2}$, and $Y_o^{\text{in}} = i(o^{\text{in}\dagger} - o^{\text{in}})/\sqrt{2}$ ($o = a_{\circ}, a_{\ominus}, m$). The linearized QLEs (11) for the quadrature fluctuations can be written as

$$\begin{aligned}
\frac{dX_{a_{\circ}}}{dt} &= (\Delta_{\circ} + G_{\circ})Y_{a_{\circ}} - \kappa_1X_{a_{\circ}} + J_1Y_{a_{\circ}}, \\
\frac{dY_{a_{\circ}}}{dt} &= -(\Delta_{\circ} + G_{\circ})X_{a_{\circ}} - \kappa_1Y_{a_{\circ}} - J_1X_{a_{\circ}} - 2G_{\circ}X_m, \\
\frac{dX_{a_{\ominus}}}{dt} &= (\Delta_{\circ} + G_{\circ})Y_{a_{\circ}} - \kappa_2X_{a_{\circ}} + J_2Y_{a_{\circ}}, \\
\frac{dY_{a_{\circ}}}{dt} &= -(\Delta_{\circ} + G_{\circ})X_{a_{\circ}} - \kappa_2Y_{a_{\circ}} + J_2X_{a_{\circ}} - 2G_{\circ}X_m, \\
\frac{dX_m}{dt} &= \Delta_m Y_m - \gamma_m X_m, \\
\frac{dY_m}{dt} &= -\Delta_m X_m - \gamma_m Y_m - 2G_{\circ}X_{a_{\circ}} - 2G_{\circ}X_{a_{\circ}}. \tag{12}
\end{aligned}$$

Then Eq. (12) can be expressed in a more concise form [50]:

$$\frac{du}{dt} = Au(t) + v(t), \tag{13}$$

where the drift matrix A reads

$$A = \begin{pmatrix} -\kappa_1 & \Delta_{\circ} + G_{\circ} & 0 & J_1 & 0 & 0 \\ -(\Delta_{\circ} + G_{\circ}) & -\kappa_1 & -J_1 & 0 & -2G_{\circ} & 0 \\ 0 & J_2 & -\kappa_2 & \Delta_{\circ} + G_{\circ} & 0 & 0 \\ -J_2 & 0 & -(\Delta_{\circ} + G_{\circ}) & -\kappa_2 & -2G_{\circ} & 0 \\ 0 & 0 & 0 & 0 & -\gamma_m & \Delta_m \\ -2G_{\circ} & 0 & -2G_{\circ} & 0 & -\Delta_m & -\gamma_m \end{pmatrix} \tag{14}$$

and $u = [X_{a_{\circ}}, Y_{a_{\circ}}, X_{a_{\ominus}}, Y_{a_{\circ}}, X_m, Y_m]^T$ and $v = [(2\kappa_1)^{1/2}X_{\circ}^{\text{in}}, (2\kappa_1)^{1/2}Y_{\circ}^{\text{in}}, (2\kappa_2)^{1/2}X_{\circ}^{\text{in}}, (2\kappa_2)^{1/2}Y_{\circ}^{\text{in}}, (2\gamma_m)^{1/2}X_m^{\text{in}}, (2\gamma_m)^{1/2}Y_m^{\text{in}}]^T$ are the vectors for quantum fluctuations and noises, respectively. Since the dynamics of the system is governed by a set of linearized QLEs, the Gaussian nature of the input states will be preserved during the time evolution. That is, the steady state of the quantum fluctuations of the system

is a CV three-mode Gaussian state. The state can be fully characterized by a stationary covariance matrix (CM) V whose matrix element is defined by [51]

$$V_{ij} = \frac{1}{2}\langle u_i(t)u_j(t') + u_j(t')u_i(t) \rangle \quad (i, j = 1, 2, \dots, 6). \tag{15}$$

The matrix V is obtained by solving the Lyapunov equation

$$\frac{dV}{dt} = A(t)V(t) + V(t)A^T(t) + D, \tag{16}$$

where $D = \text{diag}[\kappa_1(2n_{\odot} + 1), \kappa_1(2n_{\odot} + 1), \kappa_2(2n_{\odot} + 1), \kappa_2(2n_{\odot} + 1), \gamma_m(2n_m + 1), \gamma_m(2n_m + 1)]$ is a diffusion matrix whose matrix element is related to the noise correlations and defined by

$$D_{ij} = \frac{(v_i(t)v_j(t') + v_j(t')v_i(t))}{2\delta(t-t')}. \quad (17)$$

V. RESULTS AND DISCUSSION

In this section we study the enhancement of optomagnon-ics entanglement by adjusting the position of the two nanoparticles. Concretely, we introduce the definition of the logarithmic negativity between the cavity mode \hat{a}_j and the magnon mode \hat{m} in a Gaussian state. We denote the covariance matrix of the two-mode system as V' , which can be expressed as

$$V' = \begin{pmatrix} \mathcal{A} & \mathcal{C} \\ \mathcal{C}^T & \mathcal{B} \end{pmatrix}. \quad (18)$$

Here, \mathcal{A} , \mathcal{B} , and \mathcal{C} are 2×2 block forms which are related to the cavity mode, the magnon mode, and the two-mode correlation, respectively. For quantifying bipartite entanglement in a three-mode continuous-variable system, one can adopt the logarithmic negativity E_N as an effective measure; it is defined as [52,53]

$$E_N = \max[0, -\ln(2\nu^-)], \quad (19)$$

where

$$\nu^- = 2^{-1/2} \{ \Sigma(V') - [\Sigma(V')^2 - 4\det V']^{1/2} \}^{1/2}, \quad (20)$$

with $\Sigma(V') = \det \mathcal{A} + \det \mathcal{B} - 2\det \mathcal{C}$ being the smallest symplectic eigenvalue of the partial transpose of a reduced 4×4 correlation matrix V' . V' preserves the Gaussian nature, and entanglement emerges in its corresponding subsystem if and only if $\nu^- < 1/2$, which is equivalent to Simon's necessary and sufficient entanglement nonpositive partial transpose criterion (or the related Peres-Horodecki criterion) for certifying bipartite entanglement in Gaussian states [51].

Then, the *bona fide* quantification of tripartite entanglement is provided by the minimum residual contangle:

$$R_{\tau}^{ijk} = C_{iljk} - C_{ilj} - C_{ilk}, \quad (21)$$

with $i, j, k = a_{\odot}, a_{\ominus}, m$. In addition, $C_{un} = E_{un}^2$, the square logarithmic negativity with entanglement monotonicity, is the contangle of u and n subsystems, where n may involve one or two modes. The single-mode versus dual-mode logarithmic negativity is defined as

$$E_{ijk} = \max[0, -\ln(2\nu_{ijk}^-)], \quad (22)$$

where $\nu_{ijk}^- = \min \text{eig} | \oplus_{s=1}^3 (i\sigma_s \tilde{V}) |$ is the minimum symplectic eigenvalue of the 6×6 CM $\tilde{V} = P_{ijk}^- V P_{ijk}^-$. The matrices $P_{1|23} = \sigma_z \oplus \mathbb{1} \oplus \mathbb{1}$, $P_{2|13} = \mathbb{1} \oplus \sigma_z \oplus \mathbb{1}$, and $P_{3|12} = \mathbb{1} \oplus \mathbb{1} \oplus \sigma_z$ are used for partial transposition at the level of the full CM. Here, $R_{\tau}^{ijk} \geq 0$ implies that the residue contangle R_{τ} satisfies the quantum entanglement monogamy. The minimum residual contangle is defined as

$$R_{\tau}^{\min} = [R_{\tau}^{a_{\odot}|a_{\odot}m}, R_{\tau}^{a_{\odot}|a_{\ominus}m}, R_{\tau}^{m|a_{\odot}a_{\ominus}}], \quad (23)$$

which characterizes a bona fide three-party property of the CV three-mode Gaussian states. To study the bipartite CV entan-

gements, we introduce the logarithmic negativity E_N [which includes $E_{\odot\odot}(E_1)$, the CCW-CW entanglement; $E_{\odot m}(E_2)$, the CCW-magnon entanglement; and $E_{\ominus m}(E_3)$, the CW-magnon entanglement]. Further, for the tripartite entanglement, we use the minimum residual contangle given by R_{τ}^{\min} .

A. Controlled-entanglement generation via the nanoparticle

The generation of controlled entanglement strongly depends on the optical detuning $\Delta_{\odot(\ominus)}(\Delta_{1(2)})$ and the relative phase angle β . Therefore, the influence of both $\Delta_{1(2)}$ and β on bipartite entanglement is mainly discussed in the following. Specifically, in Figs. 3(a)–3(c), the logarithmic negativity E_N is plotted as a function of the scaled optical detuning $\Delta_{1(2)}$ for different values of the relative phase angle β . As demonstrated in a recent experiment [33,54], the asymmetric coupling of the two optical modes can be obtained by adjusting the positions of the two nanoparticles, and the asymmetric transmission can be realized by changing the relative phase angle. Figure 3(a) shows the dependence of entanglement on the phase angle. It is found that in the presence of the blue sideband with $\Delta_1 = -\omega_m$, E_1 presents an upward trend with the variation of β , which implies that a coherent asymmetric switch of controlled entanglement could be implemented by properly regulating the phase difference. More importantly, it is also found that the maximum value of E_1 can be enhanced 0.06 or 2 times in comparison with $\beta/\pi = 0$.

Furthermore, in terms of applying asymmetric coupling, i.e., $J_{12} \neq 0$ and $J_{21} = 0$, E_N demonstrates a complementary distribution with the variation of phase angle β . Particularly, it is shown that controlled entanglement tends to be enhanced as β approaches the EPs, implying that the nanoparticle is helpful for a quantum system to preserve its coherence. As shown in Figs. 3(d)–3(f), this result implies that, when two nanoparticles with a relative phase angle are applied to this optomagnonics system, one can entangle the optical mode and magnon mode through non-Hermitian coupling, whereas no entanglement occurs under the same parameter conditions for non-EPs cases. However, it is also seen that the degree of controlled entanglement is enhanced in comparison with the symmetric coupling. The generation of period entanglement strongly depends on the relative phase angle β and may be influenced by the imperfections of the practical materials, i.e., the optical detuning $\Delta_1 = -\omega_m$. Therefore, the influence of both Δ_1 and β on bipartite entanglement is mainly discussed in the following. First, we investigate the quantum behavior of the system without considering the relative phase angle of the nanotips β and the detuning Δ_1 . In Fig. 3(d), we find maximal entanglement (CW-CCW mode) when the optical mode is resonant with the blue sideband $\Delta_1 = -\omega_m$. As demonstrated in Fig. 3, a controlled completely asymmetric coupling of the phase angle β of two nanotips and, simultaneously, a coherent asymmetric switch of entanglement can be implemented by properly regulating the phase.

We present the results of our numerical simulations and show the bipartite entanglement as a function of the relative phase angle β and the coupling strength $G_{\odot(\ominus)}(G_{1(2)})$. All results are in the steady state guaranteed by the negative eigenvalues (real parts) of the drift matrix A . They show that a parameter regime exists around $\Delta_1 = -\omega_m$ (E_1) and

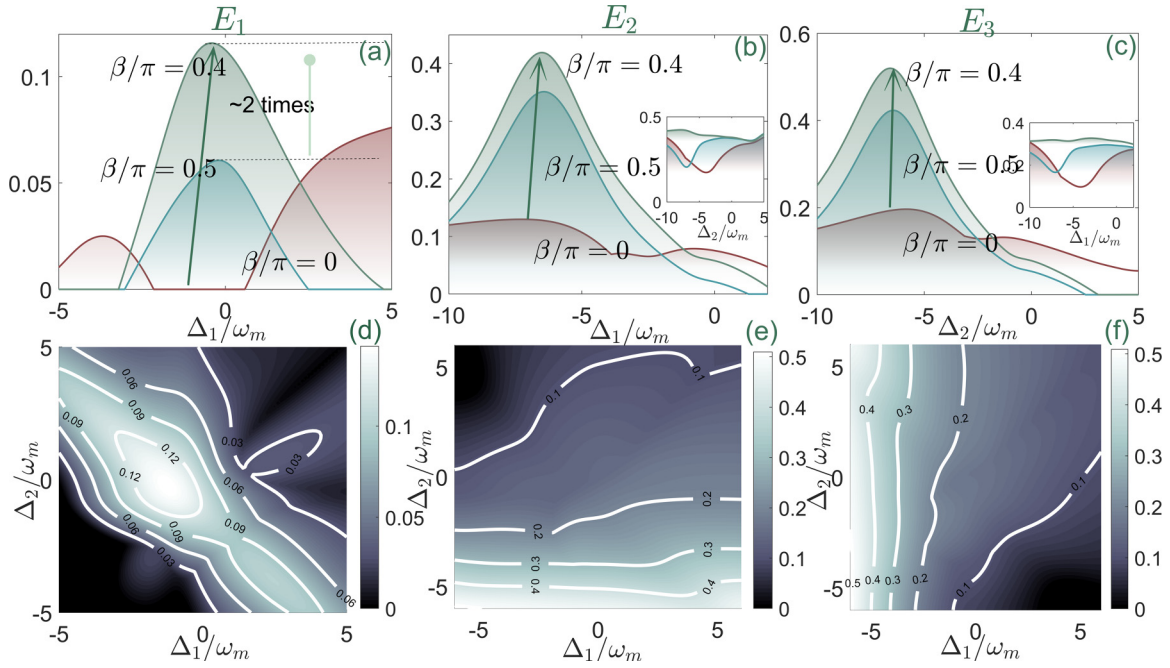


FIG. 3. Enhance of controlled entanglement between two mode (optical mode or magnon mode) due to nanoparticle mediated. Coherent asymmetric control of bipartite entanglement through tuning relative phase angle. (a)–(c) The logarithmic negativity E_N versus the optical detuning Δ for difference values of relative phase angle β . (d)–(f) The bipartite entanglement E_N changes with the optical detuning Δ_j . The parameters are set as $\kappa_1 = \kappa_2 = \gamma_m$, $G_1 = G_2 = 0.7\kappa_1$, and $\Omega = 0.1\kappa_1$.

$\Delta_{1(2)} = -5\omega_m$ ($E_{2(3)}$) where all bipartite entanglements are present. In Figs. 4(a)–4(c), we plot E_N versus the relative phase angle β . We can see that, at a finite value of the opto-

magnonics coupling strength $G_{1(2)}$, E_N reach their maximum values near the EPs. In addition, both bipartite entanglements completely vanish, i.e., $E_N = 0$ at $\beta = n\pi$, corresponding to

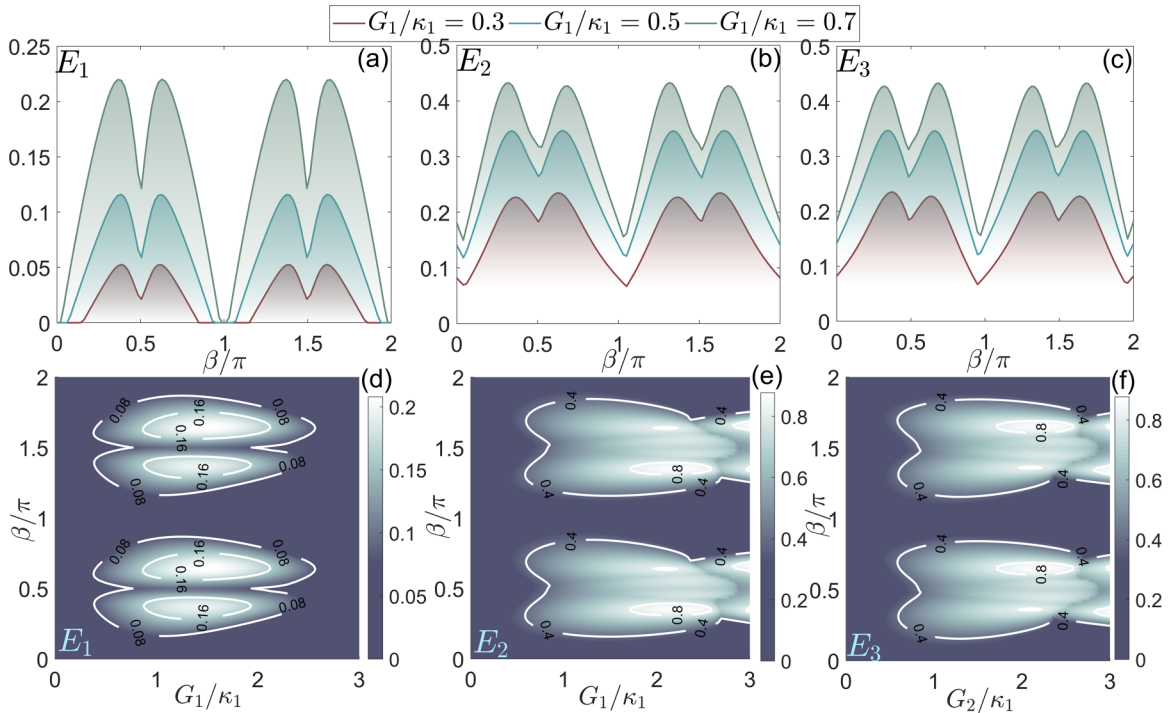


FIG. 4. By selectively adding two nanoparticles and properly adjusting their relative phase angle, the entanglement between the optical modes and magnon mode becomes periodic. (a)–(c) The logarithmic negativity E_N versus the relative phase angle β for difference values of optomagnonics coupling strength. (d)–(f) The bipartite entanglement changes with the optomagnonics coupling strength $G_{1(2)}$ and the relative phase angle β . The parameters are set as $\kappa_1 = \kappa_2 = \gamma_m$, $\Delta_{1(1)} = -\omega_m$ (E_1), $\Delta_{1(2)} = -5\omega_m$ ($E_{2(3)}$), and $\Omega = 0.1\kappa_1$.

the two nanoparticles being absent. In Fig. 4, we demonstrate how to achieve coherent periodic control of entanglement by using the non-Hermitian coupling. In the following, our aim is to obtain controlled bipartite entanglement with strong optomagnonics coupling. To demonstrate the idea, we plot in Figs. 4(d)–4(e) the entanglement changes with the optomagnonics coupling strength $G_{1(2)}$ and the relative phase angle β . By setting the threshold conditions $\Delta_1 = -\omega_m$ and $\Delta_{1(2)} = -5\omega_m$, we can obtain the optomagnonics strength $G_{1(2)}$ varying with β , which reveals the quantum behavior of the system at EPs at $\beta/\pi = 0.4$. From Fig. 4(d), we can see that photon-photon entanglement E_1 first increases and then slowly decreases with an increase of G_1 . It reaches its maximum value when $G_1/\kappa_1 = 1.5$. The photon-magnon entanglement between the CW or CCW mode and the magnon mode has a property similar to E_1 . From Figs. 4(e) and 4(f), when $G_1/\kappa_1 = 2$ and $G_2/\kappa_1 = 2$, we have entanglement $E_2 = \max[E_2]$ and $E_3 = \max[E_3]$. Therefore, photon-photon and photon-magnon entanglement can be significantly improved by selecting a suitable optomagnonics coupling strength.

B. Periodic tripartite entanglement and excitation numbers of the optomagnonics system

In the previous section, we derived the minimum residual contangle and analyzed how to control the bipartite entanglement in the optomagnonics system. Now we study in detail the tripartite optomagnonics entanglement by controlling the nanoparticles. Besides bipartite entanglement, the application of the nanoparticles can lead to controlled tripartite entanglement, as demonstrated by the nonzero minimum residual contangle in Eq. (23). In Fig. 5(a), we plot the tripartite entanglement, quantified by the minimum residual contangle R_τ^{\min} , versus the relative phase angle β . We find that in the non-Hermitian coupling regime, the tripartite entanglement is nearly twice as large as that in the non-EP regime ($\beta = \pi$). Moreover, we find from Fig. 5(b) that, when we turn off the nanoparticles (i.e., $\beta = n\pi$), the tripartite optomagnonics entanglement is strongly suppressed by the asymmetric coupling, corresponding to the emergence of the dip [dark green area in in Fig. 5(b)].

To demonstrate the conversion process, we introduce the final mean photon and magnon numbers, which can be calculated by the relation

$$N_o = \frac{1}{2}(\langle X_o^2 \rangle + \langle Y_o^2 \rangle - 1), \quad (24)$$

where $o = a_{\odot}, a_{\ominus}, m$ correspond to the excitation numbers of the CW mode, the CCW mode, and the magnon mode, respectively. Figure 6(a) presents the excitation numbers N_1 , N_2 , and N_m as a function of the two detunings of Δ_1 and Δ_2 , where two nanotip effects are considered. The numerical results are carried out in a zero-temperature environment and a weak-coupling regime, where the dissipation rate for each mode is chosen from experimentally feasible parameters. The populations of modes is caused by the interference between the energy exchange channels are shown in Figs. 3(b)–3(d), we can observe that the population of the photon modes and magnon mode completely occurs when the optical frequency detuning is negative. Because of the selection of frequency detuning and the increase of the magnon frequency, the magnon

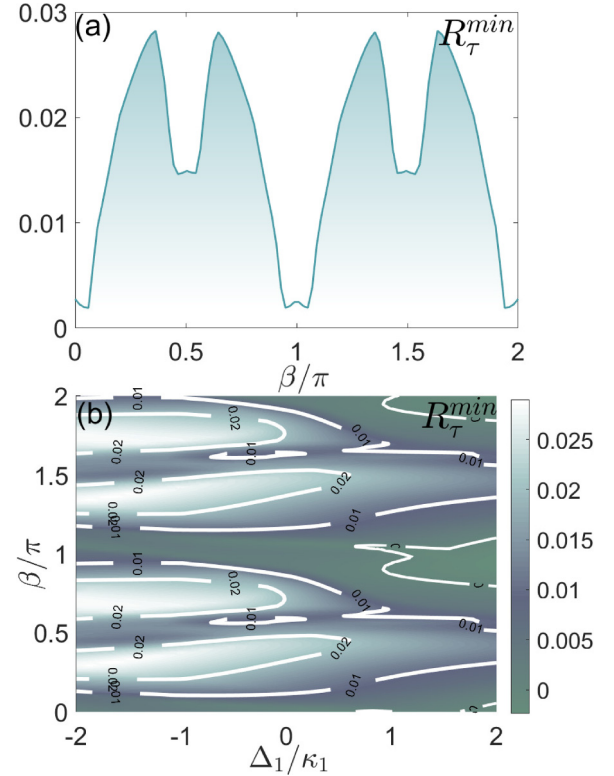


FIG. 5. (a) The tripartite entanglement R_τ^{\min} is plotted as a function of the relative phase angle β . (b) The tripartite entanglement changes with the optical detuning Δ_1 and the relative phase angle β . The parameters are set as $\kappa_1 = \kappa_2 = \kappa_m$, $\Delta_2/\omega_m = -1$, $G_1 = G_2 = 0.7\kappa_1$, and $\Omega = 0.1\kappa_1$.

and photon modes exchange energy acutely, almost all of the particles converge on one of the modes, so only one mode has significant amount of population.

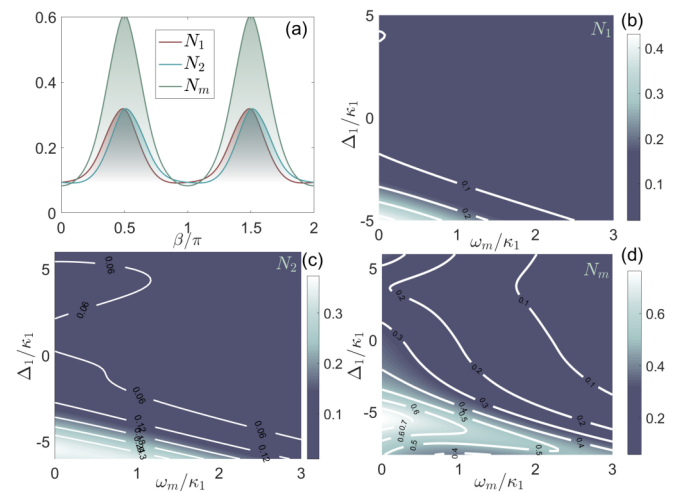


FIG. 6. (a) The excitation numbers N_1 , N_2 , and N_m as a function of the relative phase angle β . (b)–(d) The excitation numbers N_1 , N_2 , and N_m as a function of the optical detunings Δ_1 and the magnon frequency ω_m . The parameters are set as $\kappa_1 = \kappa_2 = \gamma_m$, $G_1 = G_2 = 0.7\kappa_1$, and $\Omega = 0.1\kappa_1$.

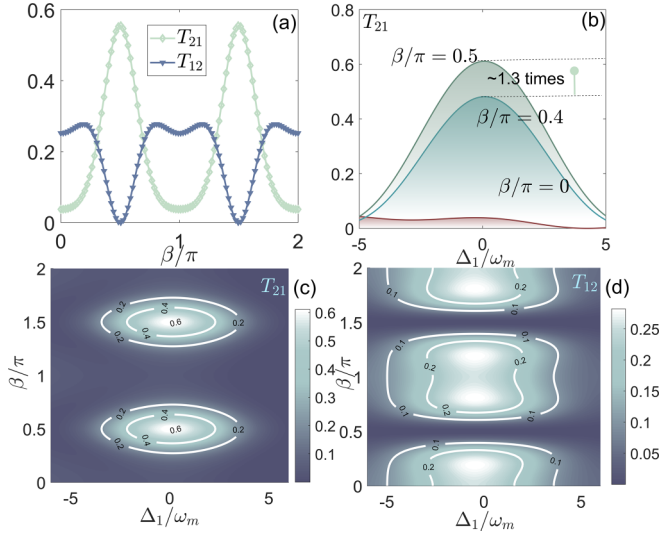


FIG. 7. Asymmetric transmission through tuning relative phase angle. (a) The asymmetric transmission $T_{21(12)}$ versus the relative phase angle β . (b) The tunable transmission T_{21} versus the optical detuning Δ_1 for different values of the relative phase angle β . (c)–(d) The asymmetric transmission $T_{21(12)}$ changes with the optical detuning Δ_1 and the relative phase angle β . The parameters are set as $\kappa_1 = \kappa_2 = \gamma_m$, $G_1 = G_2 = 0.7\kappa_1$, and $\Omega = 0.1\kappa_1$.

C. Asymmetric transmission mediated by nanoparticles

According to the input-output relation [55], we have $\hat{a}_{\text{O}}^{\text{in}} = \Omega/\sqrt{\kappa_1}$ and $\hat{a}_{\text{O}}^{\text{out}} = \sqrt{\kappa_2}\hat{a}_{\text{O}}$ for photons transmitted from optical mode \hat{a}_{O} to optical mode \hat{a}_{O} and $\hat{a}_{\text{O}}^{\text{in}} = \Omega/\sqrt{\kappa_2}$ and $\hat{a}_{\text{O}}^{\text{out}} = \sqrt{\kappa_1}\hat{a}_{\text{O}}$ for photons transmitted from optical mode \hat{a}_{O} to optical mode \hat{a}_{O} . Then the transmission coefficient from optical mode \hat{a}_{O} to optical mode \hat{a}_{O} can be defined by

$$T_{a_{\text{O}} \rightarrow a_{\text{O}}} \equiv \frac{a_{\text{O}}^{\dagger \text{out}} a_{\text{O}}^{\text{out}}}{a_{\text{O}}^{\dagger \text{in}} a_{\text{O}}^{\text{in}}} = \frac{\kappa_1 \kappa_2}{\Omega^2} \langle a_{\text{O}}^{\dagger} a_{\text{O}} \rangle,$$

$$T_{a_{\text{O}} \rightarrow a_{\text{O}}} \equiv \frac{a_{\text{O}}^{\dagger \text{out}} a_{\text{O}}^{\text{out}}}{a_{\text{O}}^{\dagger \text{in}} a_{\text{O}}^{\text{in}}} = \frac{\kappa_1 \kappa_2}{\Omega^2} \langle a_{\text{O}}^{\dagger} a_{\text{O}} \rangle. \quad (25)$$

To demonstrate tunable transmission in the hybrid cavity optomagnonics system, the transmission coefficients T_{12} and T_{21} are plotted as a function of the relative phase β in Fig. 7(a). The system shows asymmetric transmission $T_{21} \ll T_{12}$ when EPs are at $\beta = \frac{\pi}{2}$. More interestingly, Fig. 7(a) shows the β -dependent transmission rate with two nanoparticles. For $\beta = \frac{\pi}{2}$ or $\beta = \frac{3\pi}{2}$, a transparency window emerges around the optical detuning $\Delta_1 = 0$, corresponding to the frequency shifts induced by the nanoparticles. However, by tuning the system close to the EPs (with $\beta = \frac{\pi}{2}$), strong transmission can be achieved. Hence, the relative phase angle between two nanoparticles can be steered to achieve not only the chiral EPs but also the optical switching. In Fig. 7(b), we plot the tunable transmission versus the effective optical detuning Δ_1/ω_m when $\beta/\pi = 0$ (see the red solid line), $\beta/\pi = 0.4$ (see the blue solid line), and $\beta/\pi = 0.5$ (see the green solid line). More interestingly, Fig. 7(b) shows the β -dependent transmission rate with two nanoparticles due to the interference between the probe and the scattered control field. For $\beta/\pi =$

0.4 or $\beta/\pi = 0.5$, a transparency window emerges around $\Delta_1/\omega_m = 0.13$, corresponding to the frequency shifts induced by the particles. However, by tuning the system close to the EP (with $\beta/\pi = 0.4$), strong absorption of the probe can be achieved. Hence, the relative angle between two nanoparticles can be steered to achieve not only the EPs but also the optical switching. This could be of practical use in making a passive EP device for optical engineering and communications.

Moreover, we also study the effect of the parameter function on the transmission coefficient and show those results in Figs. 7(c) and 7(d). To further clarify whether asymmetric transmission can be achieved periodically by tuning the relative angle of nanoparticles, we plot the transmission coefficient as a function of the optical detuning Δ_1 and the phase angle β . The asymmetric transmission $T_{21} \ll T_{12}$ occurs at $\beta = \frac{\pi}{2}$ and $\beta = \frac{3\pi}{2}$. This result indicates that by carefully adjusting the relative phase angle of such nanoparticles, one can create nearly ideal asymmetric transmission between two optical modes. More importantly, the photons are transported one by one with high-transmission coefficients in one direction but are transported in pairs with low-transmission coefficients in the reverse direction.

VI. DISCUSSION OF THE EXPERIMENTAL IMPLEMENTATION

Recent innovative studies showed that whispering-gallery modes (WGMs) and magnon resonances can be provided simultaneously via a hybrid optomagnonic system [12]. A system providing a platform for such an interaction is a ferromagnetic sphere, supporting both optical WGMs for photons and magnetostatic (Kittel) modes for magnons. Moreover, when the nanoparticles approach the mode volume of the YIG microresonator, they perturb the evanescent fields of the counterpropagating modes and induce asymmetric coupling between them. The nanoparticles can be created experimentally by wet etching the tapered fiber, and they can be used to change the effective size and relative position of the nanoparticles [46]. With the support of the current experimental technology, the YIG sphere can be highly polished with a diameter as small as 250 μm [56], and the quality factor of the WGM optical mode is as high as 3×10^6 [16]. However, the single-crystal spherical YIG resonators can typically be manufactured with a diameter in the range of 200–1000 μm . These dimensions determine the corresponding resonant frequencies of electromagnetic modes in the sphere above 100 GHz. And the coupling constant can reach $g_j/2\pi = 2\text{--}5$ GHz. The unique properties of the cavity allow us to better utilize the high spin density of the YIG crystal for cavity QED experiments. In addition, the perturbations induced by the nanoparticles are chosen to be $\epsilon_1/\kappa = 1.5 - 0.1i$ and $\epsilon_2/\kappa = 1.485 - 0.14i$, which have been achieved experimentally [24]. Therefore, our scheme can be implemented under feasible experimental conditions.

VII. CONCLUSION

In summary, we studied the enhancement of entanglement and the manipulation of transmission between the optical photon and magnon in a nanoparticle-mediated cavity

optomagnonics system. Due to the introduction of two nanoparticles, the asymmetric backscattering of the optical-field propagation was modulated, and the optical mode exhibited strong chiral behavior in the vicinity of exceptional points. The strength of photon-photon and photon-magnon entanglement can be controlled by tuning the system toward or away from an EP and enhancing the strength of the optomagnonics coupling. We showed that the bipartite entanglement is significantly enhanced in the presence of exceptional points, which implies that a coherent asymmetric switch of controlled entanglement could be implemented by properly regulating the phase difference. By manipulating the system toward or away from EPs, versatile tunability of the tripartite entanglement, mean photon, and magnon numbers can be achieved. Additionally, the direction of asymmetric transmission can also be well tuned in a highly asymmetric way via non-Hermitian coupling. In a broader view, the ability to coherently manipulate the non-Hermitian coupling by controlling the relative phase angle of two nanoparticles could also open up a promising way to engineer various other quantum effects, such as quantum sensing, photon blockade, and slow light control. The study of controlled optomagnonics entanglement may promote the intersection and merging of various disciplines, such as non-Hermitian physics, and provide the theoretical basis and reference for the research and development of new tunable quantum devices.

ACKNOWLEDGMENTS

This work was supported by the Fundamental Research Funds for the Central Universities (Grant No. AUEA5770601223), the National Natural Science Foundation of China (NSFC; Grant No. 11675046), the Program for Innovation Research of Science at the Harbin Institute of Technology (Grant No. A201412), and the Postdoctoral Scientific Research Developmental Fund of Heilongjiang Province (Grant No. LBH-Q15060).

APPENDIX

The free Hamiltonian of the optical WGM is [12]

$$H_o = \frac{1}{2} \int \left(\varepsilon_o \mathbf{E}_i^2 + \frac{\mathbf{B}_j^2}{\mu_o} \right) d\tau, \quad (\text{A1})$$

where $\mathbf{E}_i(\mathbf{B}_j)$ is the electric (magnetic) component of the electromagnetic field inside the cavity and ε_o (μ_o) is the vacuum permittivity (permeability). By ignoring the constant term, the single-mode electromagnetic field can be quantized as $H_o = \hbar\omega_j \hat{a}_\circ^\dagger \hat{a}_\circ$, where \hat{a}_\circ (\hat{a}_\circ^\dagger) represents the annihilation (creation) operator of the j th optical mode with frequency ω_j . The free Hamiltonian of the magnon mode, including the Zeeman energy and the magnetocrystalline anisotropy energy, can be written as [11]

$$H_m = - \int \mathbf{M}_b \cdot \mathbf{B}_o d\tau - \frac{\mu_o}{2} \int \mathbf{M}_b \cdot \mathbf{H}_b^{\text{an}} d\tau, \quad (\text{A2})$$

where $\mathbf{B}_o = B_o \mathbf{e}_z$ is the static magnetic field in the z direction for magnetizing the YIG sphere, with $\mathbf{e}_{i=x,y,z}$ being the orthogonal unit vectors, and \mathbf{M}_b is the magnetization of the

Kittel mode in the YIG sphere. The anisotropic field

$$\mathbf{H}_b^{\text{an}} = \left[\frac{(2\hbar\gamma_g S_z^b K_{\text{an}})}{(\mu_o M^2 V_{\text{YIG}})} \right] \mathbf{e}_z, \quad (\text{A3})$$

where K_{an} is the dominant first-order anisotropy coefficient, M is the saturation magnetization, γ_g is the gyromagnetic ratio, V_{YIG} is the volume of the YIG sphere, and $\mathbf{S}_b \equiv (\mathbf{S}_x^b, \mathbf{S}_y^b, \mathbf{S}_z^b)$ is the collective spin operator of the Kittel mode. The Holstein-Primakoff transformations of the two modes are given by $S_z^- = S_z - m^\dagger m$, $S^+ = m\sqrt{2S - m^\dagger m}$, and $S^- = m^\dagger\sqrt{2S - m^\dagger m}$, with $S_o^\pm \equiv S_o^\pm \pm S_o^-$ [57]. Here, the macroscopic spin operator can be connected to the creation operator m^\dagger and annihilation operator m of the magnon.

We consider the coupling of the optical fields to spin-wave excitations on top of a nonuniform static ground state $\mathbf{M}_o(r)$, $\delta\mathbf{M}(r, t) = \mathbf{M}(r, t) - \mathbf{M}_o(r)$. For small deviations $|\delta\mathbf{M}| \ll 1$ we can express it in terms of harmonic oscillators (magnon modes). Quantizing $\delta\mathbf{M}(r, t) \rightarrow \frac{1}{2} \sum_\gamma [\delta\mathbf{M}_\gamma(\mathbf{r}) \hat{m}_\gamma e^{-i\omega_\gamma t} + \delta\mathbf{M}_\gamma^*(\mathbf{r}) \hat{m}_\gamma^\dagger e^{i\omega_\gamma t}]$ and $\mathbf{E}_i(\mathbf{r}, t) \rightarrow \sum_i \mathbf{E}_i(\mathbf{r}) a_i(t)$, we obtain the coupling Hamiltonian [12,15]

$$H_{mo} = \hbar \sum_{ij\gamma} S_\gamma G_{ij}^\gamma a_i^\dagger a_j + \text{H.c.}, \quad (\text{A4})$$

where

$$G_{ij}^\gamma = -\frac{i}{4} \varepsilon_o f \frac{M_s}{2} \delta \hat{m}_\gamma \cdot [\mathbf{E}_j^*(\mathbf{r}) \times \mathbf{E}_i(\mathbf{r})] \quad (\text{A5})$$

is the local optomagnonic coupling. The Greek subindices indicate the respective magnon and photon modes that are coupled. For two degenerate modes at frequency ω_j , using Eq. (A5), we observe that the frequency dependence cancels out, resulting in a simplified form for the optomagnonic Hamiltonian [12]:

$$H_{mo} = \hbar G \hat{S}_x (\hat{a}_\circ^\dagger \hat{a}_\circ + \hat{a}_\circ^\dagger \hat{a}_\circ), \quad (\text{A6})$$

with $G = \frac{1}{2} \frac{c\theta_F}{4\sqrt{\varepsilon}}$, where θ_F depends on the frequency ω , the vacuum speed of light c , and the constant f , which is related to the Faraday rotation coefficient in the material [17]. Here, ε represents the relative permittivity. We can represent the spin as a harmonic oscillator in the usual manner, with $\hat{S}_x \approx \sqrt{S/2}(m + m^\dagger)$. Using Eq. (A6), we evaluate the coupling between optical WGMs and magnon modes in a YIG sphere containing a magnetic vortex, specifically focusing on magnonic modes localized at the vortex.

In the rotating frame at the driving frequency ω_l , the Hamiltonian for the whole system can be written as

$$\begin{aligned} H_1 = & \omega_\circ \hat{a}_\circ^\dagger \hat{a}_\circ + \omega_\circ \hat{a}_\circ^\dagger \hat{a}_\circ + \omega_m \hat{m}^\dagger \hat{m} + K \hat{m}^\dagger \hat{m} \hat{m}^\dagger \hat{m} \\ & + g_1 \hat{a}_\circ^\dagger \hat{a}_\circ (\hat{m}^\dagger + \hat{m}) + g_2 \hat{a}_\circ^\dagger \hat{a}_\circ (\hat{m}^\dagger + \hat{m}) + J_{12} \hat{a}_\circ^\dagger \hat{a}_\circ \\ & + J_{21} \hat{a}_\circ \hat{a}_\circ^\dagger + \Omega (\hat{a}_\circ^\dagger e^{-i\omega_l t} + \hat{a}_\circ e^{-i\omega_l t} + \text{H.c.}). \end{aligned} \quad (\text{A7})$$

The angular frequency of the magnon mode is $\omega_m = \gamma_m B_o$, and the Kerr-nonlinear strength of the magnon mode is $K = -\hbar\mu_o\gamma_m^2 K_{\text{an}}/M^2 V_{\text{YIG}}$.

- [1] J. A. Haigh, S. Langenfeld, N. J. Lambert, J. J. Baumberg, A. J. Ramsay, A. Nunnenkamp, and A. J. Ferguson, *Phys. Rev. A* **92**, 063845 (2015).
- [2] Z. Liang, J. Li, and Y. Wu, *Phys. Rev. A* **107**, 033701 (2023).
- [3] W.-J. Wu, Y.-P. Wang, J.-Z. Wu, J. Li, and J. Q. You, *Phys. Rev. A* **104**, 023711 (2021).
- [4] X.-Y. Wu, Y. Zhang, Y.-P. Gao, and C. Wang, *Opt. Express* **29**, 40061 (2021).
- [5] Y. Nie, M. Xu, X. Zhang, M. Li, and Y. Song, *IEEE Photonics J.* **12**, 1 (2020).
- [6] Y.-P. Gao, X.-F. Liu, T.-J. Wang, C. Cao, and C. Wang, *Phys. Rev. A* **100**, 043831 (2019).
- [7] X.-L. Hei, P.-B. Li, X.-F. Pan, and F. Nori, *Phys. Rev. Lett.* **130**, 073602 (2023).
- [8] T.-X. Lu, X. Xiao, L.-S. Chen, Q. Zhang, and H. Jing, *Phys. Rev. A* **107**, 063714 (2023).
- [9] B. Zare Rameshti, S. Viola Kusminskiy, J. A. Haigh, K. Usami, D. Lachance-Quirion, Y. Nakamura, C.-M. Hu, H. X. Tang, G. E. W. Bauer, and Y. M. Blanter, *Phys. Rep.* **979**, 1 (2022).
- [10] V. A. S. V. Bittencourt, V. Feulner, and S. V. Kusminskiy, *Phys. Rev. A* **100**, 013810 (2019).
- [11] Y.-P. Wang, G.-Q. Zhang, D. Zhang, X.-Q. Luo, W. Xiong, S.-P. Wang, T.-F. Li, C.-M. Hu, and J. Q. You, *Phys. Rev. B* **94**, 224410 (2016).
- [12] S. Viola Kusminskiy, H. X. Tang, and F. Marquardt, *Phys. Rev. A* **94**, 033821 (2016).
- [13] A. Osada, A. Gloppe, R. Hisatomi, A. Noguchi, R. Yamazaki, M. Nomura, Y. Nakamura, and K. Usami, *Phys. Rev. Lett.* **120**, 133602 (2018).
- [14] Y. Ren, S. Ma, J. Xie, X. Li, and F. Li, *Opt. Express* **29**, 41399 (2021).
- [15] S. Sharma, Y. M. Blanter, and G. E. W. Bauer, *Phys. Rev. B* **96**, 094412 (2017).
- [16] X. Zhang, N. Zhu, C.-L. Zou, and H. X. Tang, *Phys. Rev. Lett.* **117**, 123605 (2016).
- [17] S. Sharma, B. Z. Rameshti, Y. M. Blanter, and G. E. W. Bauer, *Phys. Rev. B* **99**, 214423 (2019).
- [18] J. Li, S.-Y. Zhu, and G. S. Agarwal, *Phys. Rev. Lett.* **121**, 203601 (2018).
- [19] M. Peng, H. Zhang, Q. Zhang, T.-X. Lu, I. M. Mirza, and H. Jing, *Phys. Rev. A* **107**, 033507 (2023).
- [20] Y. Xiang, Y. Zuo, X.-W. Xu, R. Huang, and H. Jing, *Phys. Rev. A* **108**, 043702 (2023).
- [21] H. Lü, C. Wang, L. Yang, and H. Jing, *Phys. Rev. Appl.* **10**, 014006 (2018).
- [22] Y.-C. Tzeng, C.-Y. Ju, G.-Y. Chen, and W.-M. Huang, *Phys. Rev. Res.* **3**, 013015 (2021).
- [23] W.-L. Xu, X.-F. Liu, Y. Sun, Y.-P. Gao, T.-J. Wang, and C. Wang, *Phys. Rev. E* **101**, 012205 (2020).
- [24] W. Chen, S. K. Özdemir, G. Zhao, J. Wiersig, and L. Yang, *Nature (London)* **548**, 192 (2017).
- [25] M. Harder, Y. Yang, B. M. Yao, C. H. Yu, J. W. Rao, Y. S. Gui, R. L. Stamps, and C.-M. Hu, *Phys. Rev. Lett.* **121**, 137203 (2018).
- [26] D. Cui, J. Li, F. Li, Z.-C. Shi, and X. X. Yi, *Phys. Rev. A* **107**, 013709 (2023).
- [27] J.-X. Han, J.-L. Wu, Y. Wang, Y. Xia, Y.-Y. Jiang, and J. Song, *Phys. Rev. B* **105**, 064431 (2022).
- [28] M. Khanbekyan and S. Scheel, *Phys. Rev. A* **105**, 053711 (2022).
- [29] W. Wang, S. Liu, Z. Gu, and Y. Wang, *Phys. Rev. A* **101**, 013833 (2020).
- [30] L. Ferrier, P. Bouteyre, A. Pick, S. Cuffe, N. H. M. Dang, C. Diederichs, A. Belarouci, T. Benyattou, J. X. Zhao, R. Su, J. Xing, Q. Xiong, and H. S. Nguyen, *Phys. Rev. Lett.* **129**, 083602 (2022).
- [31] M. Kang, J. Chen, and Y. D. Chong, *Phys. Rev. A* **94**, 033834 (2016).
- [32] Z.-H. Yuan, Y.-J. Chen, J.-X. Han, J.-L. Wu, W.-Q. Li, Y. Xia, Y.-Y. Jiang, and J. Song, *Phys. Rev. B* **108**, 134409 (2023).
- [33] B. Peng, Ş. K. Özdemir, M. Liertzer, W. Chen, J. Kramer, H. Yılmaz, J. Wiersig, S. Rotter, and L. Yang, *Proc. Natl. Acad. Sci. USA* **113**, 6845 (2016).
- [34] D.-W. Wang, C. Zhao, J. Yang, Y.-T. Yan, and L. Zhou, *Phys. Rev. A* **107**, 053701 (2023).
- [35] B. Zeng and T. Yu, *Phys. Rev. Res.* **5**, 013003 (2023).
- [36] J. Wiersig, *Phys. Rev. A* **84**, 063828 (2011).
- [37] A. Banerjee and A. Narayan, *Phys. Rev. B* **102**, 205423 (2020).
- [38] J. Wiersig, *Phys. Rev. Lett.* **112**, 203901 (2014).
- [39] B. Wang, X. Jia, X.-H. Lu, and H. Xiong, *Phys. Rev. A* **105**, 053705 (2022).
- [40] T.-X. Lu, H. Zhang, Q. Zhang, and H. Jing, *Phys. Rev. A* **103**, 063708 (2021).
- [41] C. Dembowski, H.-D. Gräf, H. L. Harney, A. Heine, W. D. Heiss, H. Rehfeld, and A. Richter, *Phys. Rev. Lett.* **86**, 787 (2001).
- [42] J. Zhu, Ş. K. Özdemir, L. He, and L. Yang, *Opt. Express* **18**, 23535 (2010).
- [43] R. Huang, S. K. Özdemir, J.-Q. Liao, F. Minganti, L.-M. Kuang, F. Nori, and H. Jing, *Laser Photonics Rev.* **16**, 2100430 (2022).
- [44] L.-L. Zheng, X.-H. Xiong, X.-Y. Guo, D.-W. Zhang, and X.-Y. Lü, *Phys. Rev. A* **109**, 013502 (2024).
- [45] W. Zhang, D.-Y. Wang, C.-H. Bai, T. Wang, S. Zhang, and H.-F. Wang, *Opt. Express* **29**, 11773 (2021).
- [46] W.-L. Xu, Y.-P. Gao, C. Cao, T.-J. Wang, and C. Wang, *Phys. Rev. A* **102**, 043519 (2020).
- [47] G.-Q. Qin, X. Mao, H. Zhang, P.-Y. Wen, G.-Q. Li, D. Ruan, and G.-L. Long, *Phys. Rev. A* **106**, 063510 (2022).
- [48] T. Gao, E. Estrecho, K. Y. Bliokh, T. C. H. Liew, M. D. Fraser, S. Brodbeck, M. Kamp, C. Schneider, S. Höfling, Y. Yamamoto, F. Nori, Y. S. Kivshar, A. G. Truscott, R. G. Dall, and E. A. Ostrovskaya, *Nature (London)* **526**, 554 (2015).
- [49] S.-B. Lee, J. Yang, S. Moon, S.-Y. Lee, J.-B. Shim, S. W. Kim, J.-H. Lee, and K. An, *Phys. Rev. Lett.* **103**, 134101 (2009).
- [50] G. Adesso and F. Illuminati, *New J. Phys.* **8**, 15 (2006).
- [51] R. Simon, *Phys. Rev. Lett.* **84**, 2726 (2000).
- [52] G. Vidal and R. F. Werner, *Phys. Rev. A* **65**, 032314 (2002).
- [53] M. B. Plenio, *Phys. Rev. Lett.* **95**, 090503 (2005).
- [54] B. Peng, Ş. K. Özdemir, F. Lei, F. Monifi, M. Gianfreda, G. L. Long, S. Fan, F. Nori, C. M. Bender, and L. Yang, *Nat. Phys.* **10**, 394 (2014).
- [55] C. W. Gardiner and M. J. Collett, *Phys. Rev. A* **31**, 3761 (1985).
- [56] X. Zhang, C.-L. Zou, L. Jiang, and H. X. Tang, *Sci. Adv.* **2**, e1501286 (2016).
- [57] T. Holstein and H. Primakoff, *Phys. Rev.* **58**, 1098 (1940).